International Journal of Nanomedicine

Dovepress

open access to scientific and medical research

Open Access Full Text Article

ORIGINAL RESEARCH

Fused Deposition Modeling Printed PLA/Nano β-TCP Composite Bone Tissue Engineering Scaffolds for Promoting Osteogenic Induction Function

Wenzhao Wang[1,2,*], Pan Liu[3,*], Boqing Zhang[4], Xingyu Gui[4], Xuan Pei[5], Ping Song[2], Xia Yu[6], Zhengdong Zhang[7,8], Changchun Zhou[4]

[1]Department of Orthopaedics, Qilu Hospital of Shandong University, Shandong University Centre for Orthopaedics, Advanced Medical Research Institute, Shandong University, Jinan, Shandong, People's Republic of China; [2]Department of Orthopedics, West China Hospital of Sichuan University, Chengdu, Sichuan, People's Republic of China; [3]Hospital of Chengdu University of Traditional Chinese Medicine, Chengdu, Sichuan, People's Republic of China; [4]National Engineering Research Center for Biomaterials, College of Biomedical Engineering, Sichuan University, Chengdu, Sichuan, People's Republic of China; [5]State Key Laboratory of Biotherapy, West China Hospital, Sichuan University, Chengdu, Sichuan, People's Republic of China; [6]Department of Clinical Laboratory, Chengdu Women's and Children's Central Hospital, School of Medicine, University of Electronic Science and Technology of China, Chengdu, Sichuan, People's Republic of China; [7]School of Clinical Medicine, Chengdu Medical College, Chengdu, Sichuan, People's Republic of China; [8]Department of Orthopedics, the First Affiliated Hospital of Chengdu Medical College, Chengdu, Sichuan, 610500, People's Republic of China

*These authors contributed equally to this work

Correspondence: Xia Yu; Zhengdong Zhang, Email irisyue2021@uestc.edu.cn; doctorzzd@vip.qq.com

Purpose: Large bone defects caused by congenital defects, infections, degenerative diseases, trauma, and tumors often require personalized shapes and rapid reconstruction of the bone tissue. Three-dimensional (3D)-printed bone tissue engineering scaffolds exhibit promising application potential. Fused deposition modeling (FDM) technology can flexibly select and prepare printed biomaterials and design and fabricate bionic microstructures to promote personalized large bone defect repair. FDM-3D printing technology was used to prepare polylactic acid (PLA)/nano β-tricalcium phosphate (TCP) composite bone tissue engineering scaffolds in this study. The ability of the bone-tissue-engineered scaffold to repair bone defects was evaluated in vivo and in vitro.

Methods: PLA/nano-TCP composite bone tissue engineering scaffolds were prepared using FDM-3D printing technology. The characterization data of the scaffolds were obtained using relevant detection methods. The physical and chemical properties, biocompatibility, and in vitro osteogenic capacity of the scaffolds were investigated, and their bone repair capacity was evaluated using an in vivo animal model of rabbit femur bone defects.

Results: The FDM-printed PLA/nano β-TCP composite scaffolds exhibited good personalized porosity and shape, and their osteogenic ability, biocompatibility, and bone repair ability in vivo were superior to those of pure PLA. The merits of biodegradable PLA and bioactive nano β-TCP ceramics were combined to improve the overall biological performance of the composites.

Conclusion: The FDM-printed PLA/nano-β-TCP composite scaffold with a ratio of 7:3 exhibited good personalized porosity and shape, as well as good osteogenic ability, biocompatibility, and bone repair ability. This study provides a promising strategy for treating large bone defects.

Keywords: fused deposition modeling, PLA/nano β-TCP, composited biomaterials, large bone defect, osteoinduction

Introduction

Bone defects are the most common tissue defects observed in clinical practice. Generally, small bone defects, such as linear fractures, heal without surgical intervention, whereas larger bone defects do not heal naturally. Severe bone defects caused by congenital defects, degenerative diseases, infections, trauma, and tumors require surgical interventions, such as

Received: 6 April 2023
Accepted: 4 October 2023
Published: 17 October 2023

bone transplantation, to cure.[1,2] It is estimated that millions of patients require bone grafting each year because of large bone defects caused by various causes.[3] Autologous bone transplantation is the gold standard for bone transplantation but it has limitations such as limited donor sources, secondary trauma, easy-to-use donor site-related complications, and the inability to meet a personalized shape that matches the bone defect site.[4] Xenografts can repair bone defects in large areas but are prone to inflammation, fibrous nonunion, immune rejection, and disease transmission.[5,6] Therefore, bone tissue replacement biomaterials are urgently needed in clinical practice to improve the therapeutic effect, thus achieving the goal of reducing the treatment period and the physical, psychological, and economic burden on patients. Bone tissue engineering uses the principles and methods of tissue engineering to develop replacement materials for bone defects. Transplanting in vitro bone tissue repair materials to bone defects and achieving morphological and functional bone repair after material degradation, absorption, and bone tissue regeneration is a popular research topic.[7,8]

Polylactic acid (PLA), also known as polylactide, is a polyester polymer produced from lactic acid as the main raw material. PLA has the advantages of biosafety, biodegradability, good mechanical properties, and ease of processing and forming.[9] Moreover, PLA has good transparency, toughness, biocompatibility, and heat resistance, and has been certified by the US Food and Drug Administration as an absorbable and degradable medical material with good biocompatibility.[10] PLA is widely used in materials such as sutures, guided bone regeneration, and bioabsorbable screws.[11] PLA is also characterized by its lack of bone conduction and bone induction ability, easy-to-cause aseptic inflammatory response, and non-development under X-ray,[12,13] which lead to a limited application range of PLA 3D printing. Therefore, special processing methods or combinations with other materials are required to exploit these advantages and overcome their limitations.

Tricalcium phosphate (TCP) is a bioceramic material composed mainly of calcium and phosphorus. Its composition is similar to the inorganic composition of the bone substrate and can be divided into high-temperature α-TCP and low-temperature β-TCP according to its crystal structure.[14,15] β-TCP not only has better bone induction and bone conduction biological activities than α-TCP, but also exhibits a suitable degradation rate that matches the rate of new bone formation.[16] Animal and human cells can grow, differentiate, and reproduce normally on β-TCP materials; therefore, they are considered one of the most promising bone repair materials.[17,18] However, like many ceramic materials, β-TCP materials exhibit poor mechanical properties, high brittleness, and low bending and compressive strength. It is difficult to fix granular and powdered β-TCP after implantation into the human body, and can be easily lost.[19] The limitations of β-TCP limit its use, and recent studies have suggested its introduction into ceramic scaffolds with polymers with excellent toughness to overcome its inherent brittleness and exert its osteogenic activity.[20,21] Additionally, nano-scale β-TCP, as compared to traditional β-TCP, has smaller particles, better dispersion, and a larger surface area, and is more conducive to the biological behavior of cells.[22,23] Therefore, this study aims to use the good mechanical properties of PLA and the good bone induction and bone conduction properties of nano β-TCP by combining the two materials to prepare composite materials that fully employ their respective advantages to achieve bone repair.

With the progress in technology and processes, numerous methods to prepare bone tissue engineering scaffolds are available.[24] In recent years, 3D printing technology has shown excellent potential for providing targeted solutions to patients in the medical field because of its personalized and accurate control of the macro- and microstructures of scaffolds.[25–27] Fused deposition modeling (FDM) is used to fabricate 3D components directly from computer-aided drafting (CAD) models using filament extrusion. The material is layered by extruding the molten material onto a heated plate using a nozzle with a specified diameter. This technology allows for the rapid fabrication of bone-defect repairs with complex geometries to accommodate different bone shapes at different sites and excellent repeatability for structural customization.[28] Because FDM technology has the characteristics of fast speed, small size, ease of use, lack of pollution, and can better meet personalized needs, it has been used in the preparation of 3D scaffolds, including metal powders, ceramics, polymers, and other materials.[29,30]

FDM-3D printing technology was used to prepare PLA/nano β-TCP composite bone tissue engineering scaffolds in this study. Biodegradable PLA and bioactive β-TCP ceramics were combined to improve the overall biological performance of the composite. The results indicated that the FDM-printed PLA/nano β-TCP composite bone tissue engineering scaffolds may promote osteogenic induction function and provides a promising strategy for the treatment of large bone defects.

Materials and Methods

Synthesis of PLA/Nano β-TCP Composites

PLA (4032D) was purchased from Jinan DagangTec Company, China, and nano-scale β-TCP was purchased from DinganTec Company, China. Dichloromethane (AR) was purchased from Sinopharm Group Chemical Reagent Co Ltd, China. PLA was dissolved in dichloromethane and nano β-TCP powder was dissolved in acetone and stirred for 48 h. The two solutions were then combined, stirred, and ultrasonically dispersed for 2 h. The mixed composite liquid was volatilized at room temperature for 1 week and then dried in a vacuum drying oven at 50 °C. Our previous study found that a 70% composite ratio of PLA and ceramic materials was the optimal ratio considering their osteogenic induction ability and mechanical properties.[31] Therefore, the ratio of PLA to nano β-TCP was configured as 7:3. Finally, the PLA/nano β-TCP composite was obtained. Pure PLA was used as the control. The overall scheme of this study is illustrated in Scheme 1. The physical and chemical properties of the scaffold, biocompatibility, and in vitro osteogenic ability were comprehensively analyzed.

Preparation and Characterization of PLA/Nano-β-TCP Printing Filament

Before using the FDM-3D printer to prepare filament-like material, the prepared PLA/nano-β-TCP composite material was crushed, prepared as a composite powder, and placed in a wire drawing machine. Similar to our previous study,[32] the temperature of the material bin, extrusion temperature, and diameter were set at 175 °C, 170 °C, and 1.75 ±0.05 mm, respectively. A twin-screw extruder was used to melt and extrude the composite powder to obtain printed composite filaments for subsequent 3D printing.

FDM Fabrication and Characterization of PLA/Nano-β-TCP Scaffold

FDM printing and 3D modeling were performed as previously described.[32] 3D modeling software (SolidWorks, Dassault Systemes, France) was used to construct the print models. The STL file was output and imported into the slicing software (Simplify 3D, America). The printing parameters were set successively (printing speed was 60 mm/s and layer thickness was 0.2 mm), and the G code generated by the slicing software was exported to a secure digital card. The previously

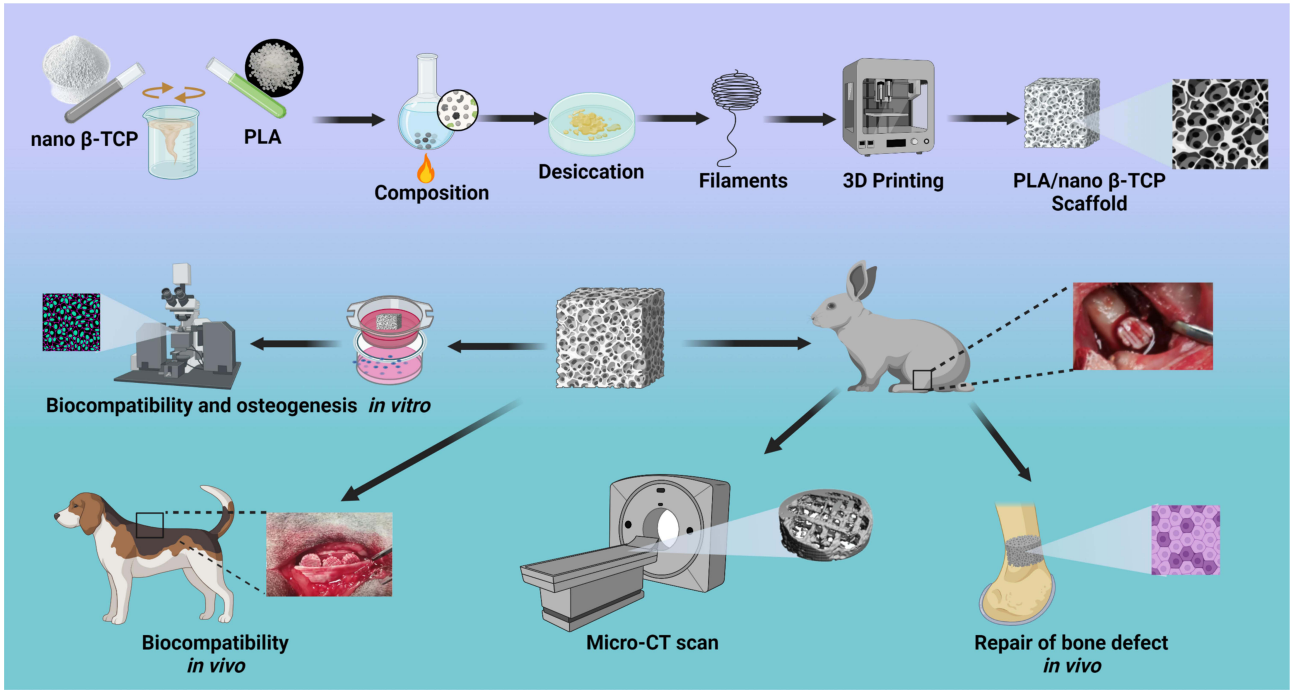

Scheme 1 Function diagram of FDM-3D-printed PLA/nano β-TCP composite bone tissue engineering scaffolds for promoting osteogenic induction.
Abbreviations: PLA, polylactic acid; β-TCP, β-tricalcium phosphate.

prepared composite filament was fed into an FDM-3D printer, and the printer then completed the solid manufacturing of the 3D model bracket according to the G code. Scanning electron microscopy (SEM; Leica, Germany) was used to examine and image the surface morphologies of the composite materials, filaments, and scaffolds. Elemental analysis of the materials was performed using energy-dispersive X-ray spectroscopy (EDS) using a Phenom™ ProX-SE Desktop (Phenomworld, Eindhoven, Netherlands). The functional groups of the materials were characterized by ATR using Fourier-transform infrared (FTIR) spectroscopy (Thermo Scientific Nicolet iS20, USA). A water contact angle (WCA) measurer (OCA20, Dataphysics, Germany) was used to measure the static contact angle of the material to determine its hydrophilicity. The mechanical properties of pure PLA and PLA/nano β-TCP cylindrical porous scaffolds were tested using a universal mechanical testing machine (CMT2103, Shenzhen, China). The cylindrical material scaffolds were 6.5 mm in diameter and 12 mm in height. Three samples were tested in each group at a test speed of 1.3 mm/min.

Double Staining of Live/Dead Cells and Fluorescence Staining Using Fluorescein Isothiocyanate (FITC)-Phalloidine

Composite scaffolds with a diameter of 1 mm were placed at the bottom of 24-well plates and rabbit bone marrow mesenchymal stem cells (BMMSCs) cultured for four generations were suspended in Dulbecco's modified Eagle's medium (HyClone, USA). The scaffolds were seeded at a concentration of 1.5×10^5 cells per scaffold, and the cell suspension was uniform. The cell suspension was then incubated for 30 min in an incubator at 37 °C and 5% CO_2. A live/dead cell double-staining kit (Abbkine, Wuhan, China) was used to evaluate the cytocompatibility of the samples. Images were collected using confocal laser scanning microscopy (CLSM; Carl Zeiss, Germany) at 1, 4, and 7 d after the experiment. The fluorescent staining kit can differentiate between living and dead cells in two colors: living cells fluoresce in green and dead cells fluoresce in red. After fixation with 4% paraformaldehyde (PFA; MultiSciences Biotech, China), the cells were permeabilized using a 0.1% Triton X-100 (Solarbo, China) phosphate buffered saline (PBS, 0.01 M, pH = 7.4) solution for 15 min and washed with PBS three times. The cytoskeleton was stained using FITC-phalloidine (Abbkine, Wuhan, China) in the dark for 30 min, followed by staining of the nucleus using 4′,6-diamidino-2-phenylindole (DAPI; 10 μg/mL, Abbkine, Wuhan, China) at room temperature for 30s. CLSM was used for observation and imaging (1, 4, and 7 d after the experiment).

Osteogenic Differentiation Staining

MC3T3-E1 cells (Zhong Qiao Xin Zhou Biotechnology Co., Ltd, Shanghai, China) were implanted in the lower chamber of a transwell plate (Corning, Chengdu, China) and cultured in an incubator at 37 °C and 5% CO_2 after adding an α-MEM (HyClone, USA) complete culture medium. When the cell density covered approximately 60–70% of the lower compartment area, a scaffold was placed in the upper chamber of the transwell plate and replaced with an osteogenic medium prepared with 10 nM dexamethasone (Solarbio, China), 50 μg/mL vitamin C (Solarbio, China), and 10 nM β-glycerolphosphate (Solarbio, China). Subsequently, they were cultured in incubators at 37 °C and 5% CO_2, and the osteogenic induction medium was changed every 48 h. MC3T3-E1 cells were co-cultured with the two groups of scaffolds in different transwell chambers. After removing the medium, the samples were washed three times with PBS, fixed in 4% PFA for 20 min, and washed again with PBS. Images were acquired after staining at room temperature in the dark using an alkaline phosphatase (ALP) assay kit (Beyotime Biotechnology, Shanghai, China) according to the manufacturer's instructions (at 4 and 7 d after the experiment). MC3T3-E1 cells were co-cultured with the two groups of scaffolds in different transwell chambers. Samples were fixed in 4% PFA for 20 min, washed in PBS three times, PBS was discarded, and 0.2% Alizarin Red S (Solarbio, China) prepared using Tris-HCl (pH = 6.0) was added and stained at room temperature for 30 min. The mixture was washed three times with deionized water. Calcium nodule formation was evaluated after images were collected under an inverted microscope (Carl Zeiss, Germany) (at 14 and 28 d after the experiment).

Immunofluorescence Detection

MC3T3-E1 cells were co-cultured with the two scaffolds for 7 d. The samples were fixed in 4% PFA for 5 min, washed with PBS three times, PBS was discarded, and the cells were then treated with a 0.1% Triton X-100 PBS solution for 15

min. The cells were then incubated in PBS containing 4% goat serum for 30 min. The cells were then treated with anti-osteocalcin (OCN) antibodies (1:100, ServiceBio, Wuhan, China) and anti-collagen I (COL1) antibodies (1:500, Abcam, ab 21286, UK) an incubated overnight at 4 °C. The cells were washed three times with 0.1% Tween 20 in PBS three times and incubated at room temperature with a secondary antibody for 50 min. The nuclei were stained with DAPI (10 μg/mL) for 10 min. The images were captured using a fluorescence microscope.

Animal Experimentation in vivo

Four healthy beagles (10–11 kg, male) were randomly divided into two groups. After intraperitoneal injection of pentobarbital anesthesia, the back hair was shaved, conventional disinfection was performed, and a longitudinal incision of approximately 2–3 cm was made on the skin near the spine, which was separated layer-by-layer from the muscle. The two stents were implanted into the muscle layers of the different groups of beagles and the incisions were conventionally sutured. After recovery from anesthesia, the animals were placed in cages to continue feeding. Four weeks after surgery, euthanasia was performed. The stent implanted in the muscle layer was dissected and recovered, and then fixed in a formalin solution. After dehydration, the samples in both groups were not decalcified and hard tissue sections were prepared after embedding in paraffin. Hematoxylin and eosin (H&E) staining (Solarbio, Beijing, China) was performed using a microscope. Twelve healthy normal-grade New Zealand white rabbits (male; body weight of 2–3 kg) were divided into two groups (six rabbits per group). After intravenous anesthesia with 3% (m/v) pentobarbital was administered at a dose of 30 mg/kg, the animal was fixed on the operating table, the hair of the lower extremities was shaved, and the towel was routinely disinfected. An approximately 2 cm-long longitudinal incision was made in the middle and lower thigh, the muscles and fascia were carefully separated until the femoral shaft was exposed, and the femoral shaft was drilled using a 5 mm-internal diameter trephine to create a bone defect model. The sterilized FDM-3D printed PLA/nano β-TCP composite and pure PLA scaffolds were implanted in the different groups of rabbit femurs. No muscle or other soft tissue was embedded in the bone defect. After correctly aligning the stent, the soft tissue and skin of the incision were sutured without tension. After awakening from anesthesia, the animals were returned to their cages for further feeding. The animals were euthanized after 4 weeks, and the bone defect samples were scanned using micro-computed tomography (micro-CT, PerkinElmer, USA). The samples were placed in a 10% decalcified solution of ethylenediaminetetraacetic acid (Solarbio, Beijing, China) for six months, after which successful decalcification was verified using the acupuncture method. The 75, 85, and 90% gradient alcohols were dehydrated for 5 min each and the embedding of paraffin was followed by a 5 μm-thick section mechanism. H&E and Masson's trichrome staining (Solarbio, Beijing, China) were performed. All animal experiments were approved by the Ethics Committee of Sichuan University (approval number:20220304050) in accordance with the Guidelines for the Ethical Review of Laboratory Animal Welfare (GB/T 35892–2018) and ARRIVE 2.0.

Statistical Analysis

Statistical analyses were performed using GraphPad Prism 9.0.0 software. The data was expressed as a mean ± standard deviation, and an independent sample *t*-test was used to compare the two groups. Statistical significance was set at $P < 0.05$.

Results

SEM and Raw Materials Composition Analyses

The nano-scale β-TCP particles were observed using SEM. The sizes of the nano-scale β-TCP particles were uniform, the binding was tight, and a small quantity of the particles were dispersed (Figure 1A-C). The distribution of nano β-TCP particles were determined using EDS analyses. The results showed that the calcium content was the highest, followed by phosphorus and oxygen (Figure 1D-G). Nano-scale β-TCP (Figure 1H) was mixed with dichloromethane, acetone, and PLA to form a composite solution (Figure 1I), which was then dried to obtain composite blocks (Figure 1J) and further crushed to obtain composite particles (Figure 1K). The PLA and composite materials were processed into 1.75 mm-diameter filaments (Figure 1L and M). Using FDM 3D printing, scaffolds with different internal pores and external structures were obtained by adjusting the printing parameters to achieve personalized production (Figure 1N and O).

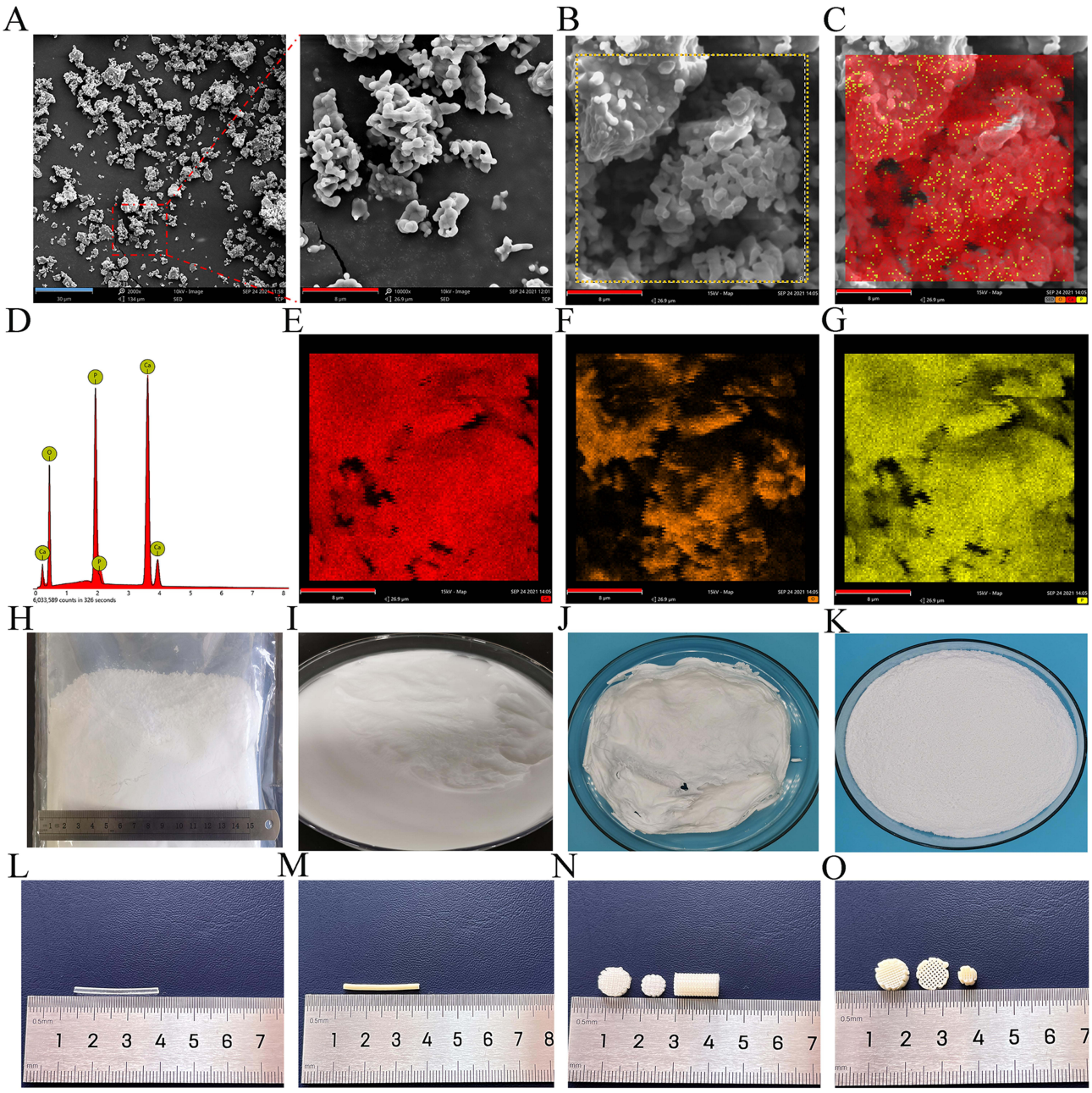

Figure 1 Material morphology and detection. (**A**) SEM images of the nano β-TCP particles showing the uniform size of the nano-sized particles (blue bar = 30 μm, red bar = 8 μm). (**B-G**) Elemental analysis of the nano β-TCP particles, where red represents calcium (**E**), Orange represents oxygen (**F**), and yellow represents phosphorus (**G**). Nano β-TCP particles in natural light (**H**). PLA/nano β-TCP composite solution (**I**), block (**J**), and particles (**K**). Pure PLA filament (**L**) and PLA/nano β-TCP composite filament (**M**). FDM-3D-printed PLA scaffolds (**N**) and PLA/nano β-TCP composite scaffolds (**O**).
Abbreviations: β-TCP, β-tricalcium phosphate; SEM, scanning electron microscopy; PLA, polylactic acid; FDM, Fused deposition modeling.

Morphology and Structure Characterization of Filaments and Scaffolds

The pure PLA filament was smooth with slight protrusions. However, due to the addition of nano β-TCP to the PLA/nano β-TCP composite filament, its surface was rough and had a uniform particle distribution and exhibited a loose porous structure, which will increase its surface area to facilitate cell adhesion. The pores of the two groups of scaffolds were 300–400 μm in size, clear and, orderly distributed. The surface morphology was consistent with that of the filament (Figure 2). The FTIR results showed that the spectral bands at 1082, 1747, and 2996 in the PLA spectrum corresponded to C-O, C=O, and C-H stretching, respectively. The nano β-TCP spectrum exhibited absorption bands at 548, 606, and 1042, which were attributed to the phosphate (PO_4^{3-}) groups. 3449 functional groups derived from water molecules

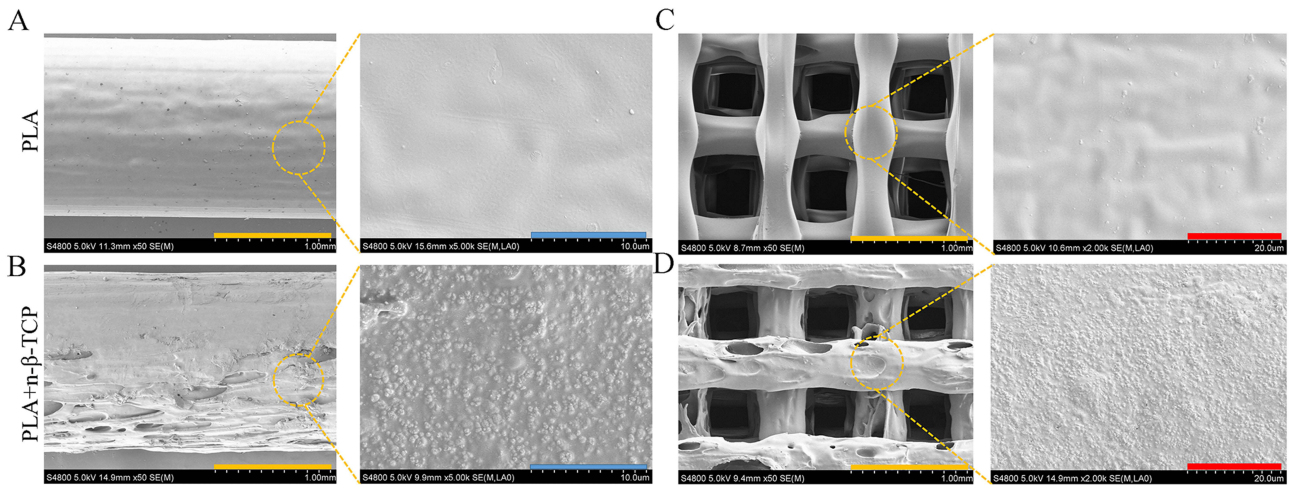

Figure 2 Filament and FDM-3D-printed scaffold. (**A** and **B**) SEM images of the morphology of the filament (yellow bar = 1 mm, blue bar = 10 μm). (**A**) The surface of the pure PLA filament was smooth with slight protrusions and (**B**) the surface of the PLA/nano β-TCP composite filament was rough and the particles were evenly distributed. (**C** and **D**) SEM images of the morphologies of the scaffolds (yellow bar = 1 mm, blue bar = 20 μm). The two scaffolds had clear pores and regular vertical and horizontal arrangements. (**C**) The surface of the pure PLA scaffold was smooth and (**D**) the surface of the PLA/nano β-TCP composite scaffold was rough with uniform particles.
Abbreviations: SEM, scanning electron microscopy; PLA, polylactic acid; β-TCP: β-tricalcium phosphate.

(OH^-). The PLA/nano β-TCP composites exhibited typical PLA bands and absorption bands of PO_4^{3-} and water molecules, confirming the presence of nano-β-TCP particles in the PLA matrix (Figure 3). The WCA of pure PLA was 86.33 ±0.64°, whereas that of PLA/nano β-TCP was 76.8 ±1.81°. The surface roughness of the PLA/nano β-TCP composite material, as compared with that of pure PLA, increased and its hydrophilicity improved (Figure 4A). The compressive mechanical properties of the scaffolds suggested that the pure PLA scaffold could maintain its structural integrity after the pressure test, whereas the PLA/nano β-TCP composite scaffold exhibited slight yielding (Figure S1). The mechanical test results indicated that the compressive strength of the PLA/nano β-TCP composite scaffolds was lower than that of the pure PLA scaffolds (Figures 4B and S1).

Biocompatibility

The PLA/nano β-TCP composite scaffold loaded with rabbit BMMSCs was observed using SEM, revealing that the rabbit BMMSCs attached to the surface of the PLA/nano β-TCP composite scaffold grew normally and the cells were spindle- or polygonal-shaped with a natural morphology (Figure 5A). A live/dead cell double-staining kit was used to stain the BMMSCs on the scaffold on the 1st, 3rd, and 7th days, respectively. Almost all rabbit BMMSCs on the PLA/

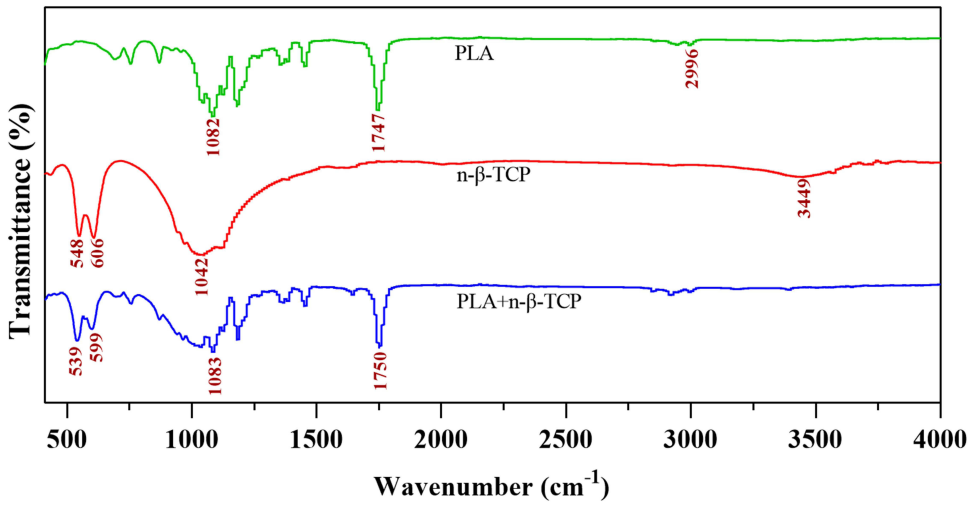

Figure 3 FTIR spectra of PLA, nano β-TCP, and PLA/nano β-TCP.
Abbreviations: FTIR, Fourier transform infrared; PLA, polylactic acid; β-TCP, β-tricalcium phosphate.

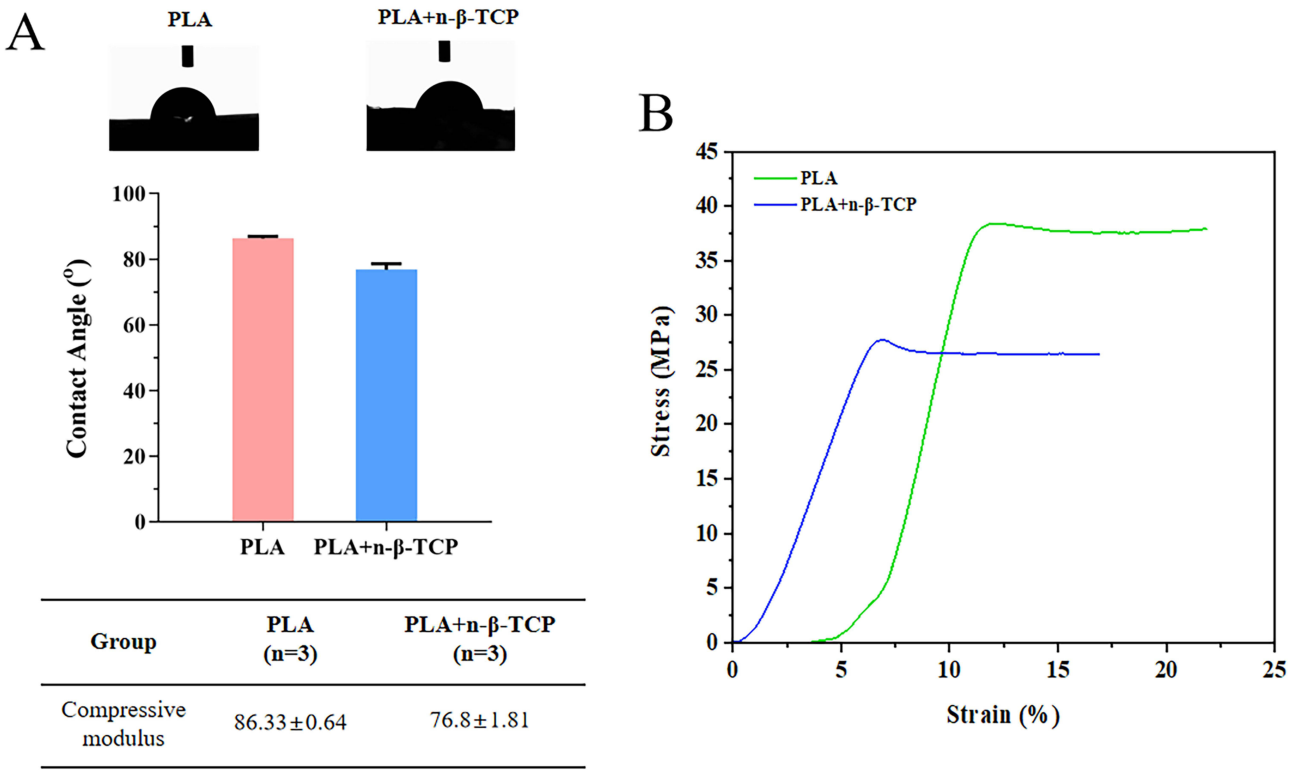

Group	PLA (n=3)	PLA+n-β-TCP (n=3)
Compressive modulus	86.33±0.64	76.8±1.81

Figure 4 WCA and mechanical properties of the two scaffold groups. (**A**) WCA and (**B**) stress-strain curves of the two scaffold groups.
Abbreviation: WCA: Water Contact Angle Measurement.

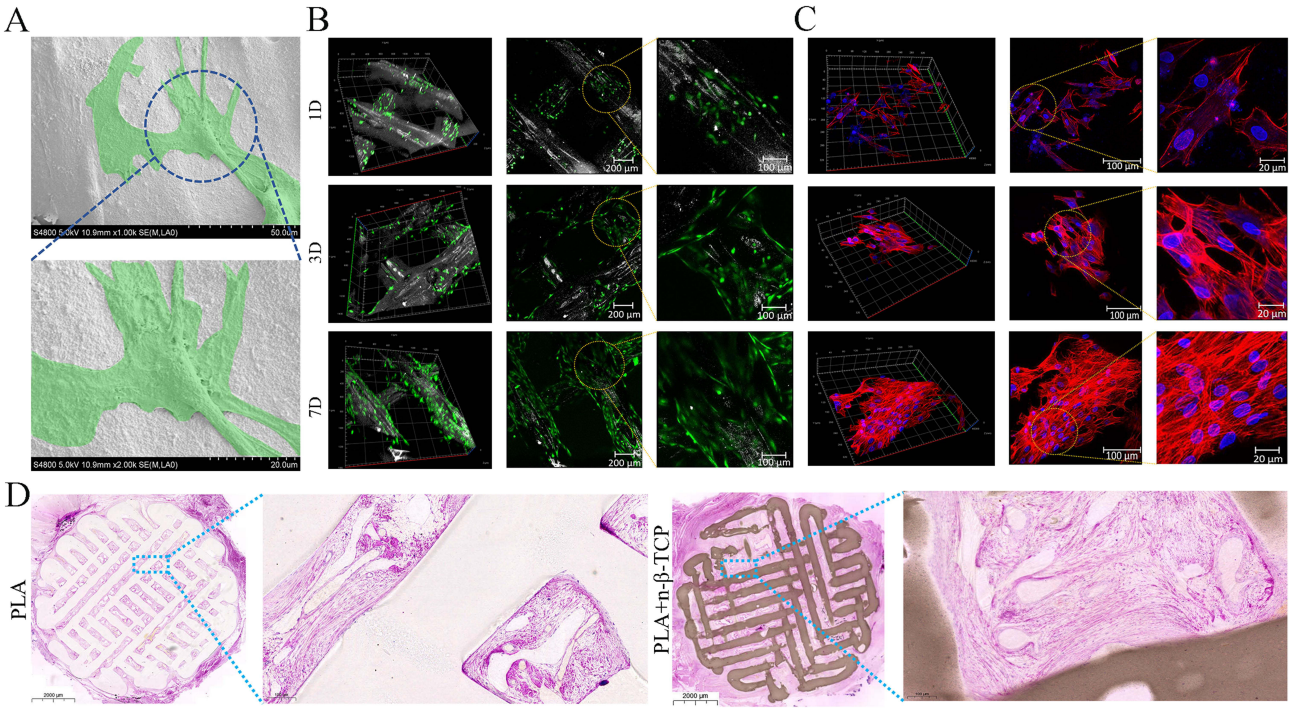

Figure 5 Biocompatibility of the FDM-3D-printed scaffolds. SEM image of the PLA/nano β-TCP composite scaffold loaded with rabbit BMMSCs: (**A**) the cells are marked in the green area and were observed to be stretched out and normally attached to the surface of the scaffold. Live/dead cells double staining (**B**) and fluorescence staining of FITC-phalloidine (**C**) were performed on the scaffold loaded with rabbit BMMSCs on the 1st, 3rd, and 7th days. Cells proliferated and spread on the surface of the PLA/nano β-TCP composite scaffold. (**D**) Pure PLA scaffolds and PLA/nano β-TCP composite scaffolds were implanted into the back muscle of beagle dogs for 4 weeks and hard tissue sections were stained with H&E. Muscle tissue filled both scaffolds and no inflammatory cell proliferation was observed.
Abbreviations: FDM, Fused deposition modeling; SEM, scanning electron microscopy; PLA, polylactic acid; β-TCP, β-tricalcium phosphate; BMMSCs, bone marrow mesenchymal stem cells; FITC, fluorescein isothiocyanate; H&E, Hematoxylin and eosin.

nano β-TCP composite scaffold were living cells, as determined using CLSM, and no obvious red dead cells were observed. The BMMSCs on PLA/nano β-TCP composite scaffolds on day 7 were densely distributed with green fluorescence and the number of BMMSCs increased significantly, showing good cytocompatibility (Figure 5B). F-actin is a cytoskeletal protein that can be used to analyze the cytocompatibility of composite scaffolds by evaluating the microfilament morphology of F-actin in cells. Based on the CLSM observations, the cells exhibited a polygonal spread under the support of ordered F-actin and no obvious nuclear abnormalities were observed. The cells extended, adhered, and proliferated on the surface of the PLA/nano β-TCP composite scaffold with an increasing incubation time (Figure 5C). When samples were acquired from the back paravertebral muscles of the beagle dogs, both groups of animals were observed to have healed back surgical incisions without necrosis, inflammation, or exudation. At the time of tissue dissection, no serious inflammatory reactions or pus were observed around the implanted samples. H&E staining was performed on hard tissue sections of the extracted specimens for histological evaluation. The scaffolds in the pure PLA group were observed to be transparent, whereas those in the PLA/nano β-TCP group were brown. The scaffolds in both groups were filled with muscle tissue and no proliferation of inflammatory cells was observed (Figure 5D).

Testing of Osteogenic Capacity in vitro

The osteogenic induction ability is an important indicator for evaluating in situ bone repair scaffolds, and ALP is considered an important marker of the osteogenic differentiation of cells. After the MC3T3-E1 cells were co-cultured with the two groups of scaffolds, little difference in the ALP staining color was observed between the two groups on day 4. The staining of the pure PLA/nano β-TCP composite scaffold group on day 7 was significantly deeper than that of the PLA scaffold group, showing higher ALP activity (Figure 6A). The results of the Alizarin Red staining of the MC3T3-E1 cells were similar after 14 d of co-culture with the two scaffold groups under the intervention of osteogenic inducers. On day 28, the number of calcium nodules formed in the PLA/nano β-TCP composite scaffold group increased significantly, the diameter increased, the color of calcium salt deposition was darker, and the number of calcium nodules formed in the PLA/nano β-TCP composite scaffold group was significantly greater than that in the pure PLA scaffold group, showing a stronger osteogenic ability (Figure 6B). OCN is a bone-specific protein synthesized by osteoblasts during the matrix mineralization stage, and is regarded as a marker of osteoblast differentiation and maturation. Immunofluorescence staining of OCN was performed on MC3T3-E1 cells, and the expression of the OCN protein (red) in the PLA/nano β-TCP composite scaffold group was significantly higher than that in the pure PLA scaffold group. Furthermore, immunofluorescence staining revealed that the expression of the COL1 protein (green) in MC3T3-E1 cells in the PLA/nano β-TCP composite scaffold group was significantly higher than that in the pure PLA scaffold group on day 7 (Figure 6C).

In vivo Evaluation of Bone Defect Model

H&E staining showed that the scaffolds in both groups were filled with well-positioned bone defects without displacement. A very small quantity of new sporadic bone formation was observed in the pure-PLA group. The scaffolds were not tightly bound to the new bone, and defects in the bone tissue remained evident. In the PLA/nano β-TCP composite scaffold group, a large number of new bones were formed around the scaffold, the scaffold was closely combined with the bone tissue, a large quantity of new bone was filled in the scaffold material, and the thickness of the new bone trabecula was good (Figure 7A). In the pure PLA group, a small amount of new bone and collagen fibers was formed and the scaffold was not tightly bound to the collagen or new bone, resulting in obvious bone defects. In the PLA/nano β-TCP composite scaffold, new bone was observed around the scaffold, a large quantity of collagen content was observed, which was significantly higher than that in the pure PLA scaffold group, and the scaffold was closely combined with bone tissue (Figure 7B). Evaluation of the bone defect site showed that there was almost no new bone formation in the bone marrow cavity of the pure PLA group, whereas a large quantity of new bone was formed in the bone marrow cavity of the PLA/nano β-TCP composite scaffold group and a large quantity of new bone was wrapped around the scaffold (Figure 7C). The micro-CT analysis and H&E staining results indicated that the new bone grew from the

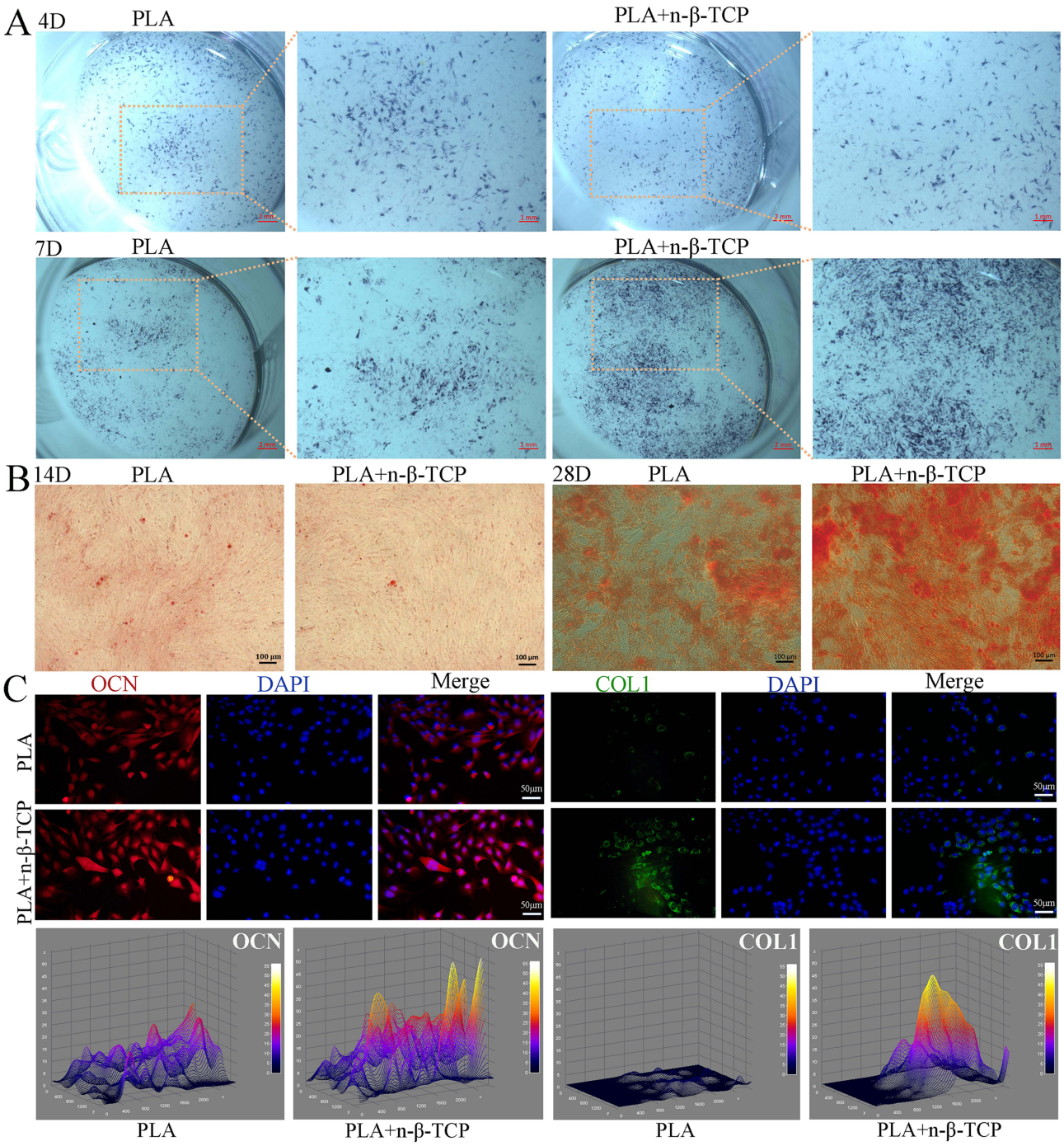

Figure 6 MC3T3-E1 cells were co-cultured with scaffolds from both groups and osteogenesis was induced in vitro. (**A**) MC3T3-E1 cells co-cultured with the two scaffolds were stained with ALP on days 4 and 7 after osteogenic induction. (**B**) MC3T3-E1 cells co-cultured with the two scaffolds were stained with Alizarin Red on days 14 and 28 after osteogenic induction. (**C**) The expression of osteogenic markers (OCN, COL1) was detected using immunofluorescence on the 7th day after osteogenesis induced by the co-culture of MC3T3-E1 cells with the two scaffold groups.

Abbreviations: ALP, Alkaline phosphatase; OCN, osteocalcin; COL1, anti-collagen I.

edge of the bone defect inward towards the middle. The mineral density (MD) and bone tissue volume (BV)/total volume (TV) values of the femur defect sites were calculated and analyzed using the SCANCO Medical System software. The MD and BV/TV values of the PLA/nano β-TCP composite stent group were found to be significantly higher than those of the pure PLA group, and the difference was statistically significant ($P < 0.05$) (Figure 7D and E).

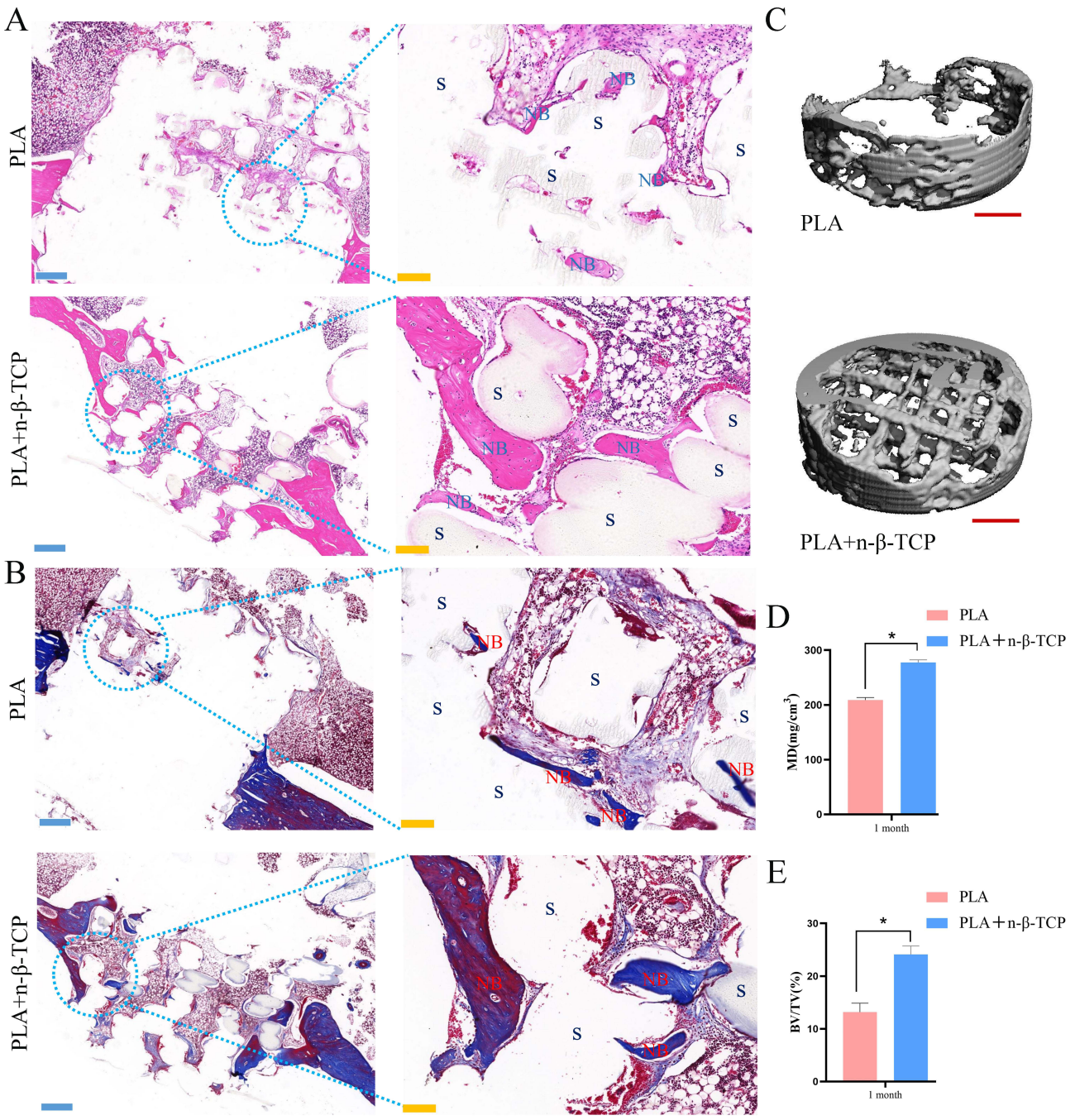

Figure 7 Osteogenesis of two groups of scaffolds observed in vivo. Samples from the two scaffold groups were taken 1 month after stent implantation in the rabbit femur bone defect model. After decalcification, sections were sliced for H&E (**A**) and Masson staining (**B**), with S representing the scaffold and NB representing the new bone. (**C**) 3D reconstruction of the micro-CT scans performed on the implantation areas of the two scaffold groups. (**D**) The MD and (**E**) BV/TV were analyzed. *, $p < 0.05$.
Abbreviations: H&E, Hematoxylin and eosin; Micro-CT, micro-computed tomography; MD, mineral density; BV, bone tissue volume; TV, total volume; NB, new bone.

Discussion

An ideal tissue engineering bone repair material should have good mechanical properties, biocompatibility, osteoconductivity, osteoinductivity, a wide range of source materials, and simple preparation to meet the functional requirements of materials for clinical application.[33,34] With increasing research on bone repair materials, it is difficult for a single material to meet the above conditions. Composites that optimally combine two or more materials with different properties have attracted considerable attention. Previous studies have shown that the preparation of composite scaffolds

with better biological activity and biomimetic structures using a combination of materials is theoretically feasible and have achieved some preliminary results.[32,35,36] Composite scaffolds can compensate for the deficiency of a single material; therefore, their performance advantages and disadvantages are complementary for better alignment with the needs of bone tissue engineering scaffolds materials.[37] β-TCP is widely used in stomatology, bone tissue engineering, and orthopedics because of its excellent osteoconductivity and osteoinductivity.[38] However, the brittleness and poor mechanical properties of porous β-TCP limit its application.[17,39] PLA also has limitations owing to its lack of osteoconductivity and osteoinductivity, poor mechanical properties, and easy aseptic inflammatory response.[31,32] Composite scaffolds were fabricated in this study using PLA and nano β-TCP to fully complement their advantages and disadvantages for bone defect repair. PLA and nano β-TCP were used to prepare composite filaments, perform FDM-3D printing to fabricate composite scaffolds, and perform in vitro and in vivo studies on the biocompatibility and osteogenic properties. Apatite in human bone is distributed in needle-like nanoscale patterns, and nanoparticles have better biological activity and osteoconductivity than microparticles, which is conducive to bone integration at the bone-implant interface.[40,41] Therefore, the preparation of nano-scale β-TCPs is important. The results of this study showed that the nano-scale β-TCP particles were homogeneous and contained higher amounts of calcium and phosphorus, which are required for osteogenesis.

Studies have confirmed that a material with a rough surface is more conducive to cell attachment.[42] Our previous study found that a 30% combination ratio of bioceramic materials (for example, nanohydroxyapatite) with PLA was an ideal ratio that not only met the mechanical strength requirements, but also promoted the osteogenic effect.[43] However, when the proportion of bioceramics was > 50%, the composite material could not continuously and stably pass through the printing nozzle owing to its high brittleness, which led to difficulties in preparing the composite material.[32] In this study, the filament and composite scaffolds prepared using FDM-3D printing with a PLA:nano β-TCP ratio of 7:3 exhibited rough surfaces without cracks, and the uniform distribution of particles was conducive to cell adhesion. The WCA results also confirmed that the hydrophilicity of the PLA/nano β-TCP composite was better than that of pure PLA and was more conducive to cell adhesion to promote bone formation. The porosity of bone-repair materials is an important factor for enhancing the material used in the bone-reconstruction process. An ideal scaffold should have a network of interconnected pores to promote the exchange of oxygen, nutrients, and waste and promote the growth of cells into the scaffold.[44,45] Pores in the 75–100 μm range generally promote bone mineralization, but such pores are easily blocked and can be penetrated by fibrous tissue and interfere with the repair,[46] whereas large pores often do not ensure mechanical support of the scaffold. Therefore, a scaffold pore size of 200–400 μm is more suitable.[35] Previous studies have shown that it is difficult to control the pore size of PLA/nano β-TCP composite scaffolds prepared using electrospinning, rapid volume expansion phase separation, and freeze-drying.[47] The pore size of the scaffold material prepared in this study was 300–400 μm. The pores of the two material scaffold groups were clear and connected to each other, which was conducive for the exchange of substances and cell growth.

The characteristics of PLA and its low glass transition temperature (Tg) (55–65 °C) make it deformable at a high melting temperature (Tm) (170–180 °C) for facile conversion into filaments.[11,48] Lou et al found that the high temperature of the sintering method of approximately 175 °C more evenly distributed the β-TCP powder on the surface of the PLA fiber; however, it also isolated the pores in the material scaffolds.[49] Elhattab et al used FDM to 3D-print composite β-TCP/PLA filaments and demonstrated that the filaments could be printed at a maximum nozzle temperature of 220 °C; however, its degree of crystallinity increased.[50] The extrusion temperature of FDM-3D printing in this study was set to 170 °C to obtain a good uniform distribution effect of nano β-TCP powder on the surface of the composite scaffolds. This characteristic was confirmed using FTIR spectroscopy. An ideal scaffold should have good physiological compatibility, which means that the material can be safely used in the human body, including supporting normal cell activities, not producing toxicity to attached cells and tissues, not being rejected, and not causing chronic infection.[51,52] Rabbit BMMSCs were used for in vitro culture and it was observed that rabbit BMMSCs adhered well on the PLA/nano β-TCP composite scaffold. The results of the live/dead cell double staining and FITC-phalloidin fluorescence staining showed that the composite scaffolds exhibited good biocompatibility and were nontoxic to cells. A biocompatibility test of the scaffolds implanted into the back muscles of beagle dogs in vivo showed that the two groups of scaffolds had good biocompatibility, no inflammation or infection occurred, and no obvious heterotopic ossification occurred. As mentioned

above, the acid degradation of PLA produced by in vivo degradation may lead to an inflammatory reaction;[53,54] however, nano β-TCP and its compound preparation may play an inhibitory role in this inflammatory reaction. This is a key process for bone regeneration in the design of scaffolds for observing their osteogenic capacity and promoting the repair of bone defects.

Owing to the poor effect of the relevant immune antibodies being superior to those of rabbit origin, MC3T3-E1 cells were uniformly used in the in vitro osteogenic experiments. The ALP and Alizarin Red staining results showed that osteoblast differentiation in the PLA/nano β-TCP composite scaffold group was significantly higher than that in the pure PLA scaffold group. OCN is essential for bone matrix mineralization and COL1 is important for bone formation and participates in many physiological processes, such as biological adaptation and tissue regeneration.[55,56] COL1 is the most abundant component of bone organic matter, accounting for more than 90% of the bone organic matter, and is essential for the development, formation, and homeostasis of bone tissue, maintenance of the bone structure integrity, and biomechanical properties of bone.[57] The results of this study showed that the expression of OCN and COL1 in MC3T3-E1 cells in the composite scaffold group was significantly higher than that in the pure PLA group, indicating that the PLA/nano β-TCP composite scaffold was more conducive to the osteogenic differentiation of MC3T3-E1 cells. Therefore, the PLA/nano β-TCP composite scaffold has better osteoconductivity and osteoinductivity.

Previous studies have shown that PLA and β-TCP have attracted the interest of researchers as bone-repair materials. Neither PLA nor β-TCP alone can achieve a good match for new bone formation and affect bone defect repair.[58–60] Cao et al used a PLA/nβ-TCP interbody fusion cage with greater biomechanical stability in implants for single-level cervical fusion in goats, and reported an increase in the BV/TV ratio and better interbody fusion than the fusion in an autograft to the anterior iliac ridge using polyetheretherketone (PEEK) cages.[61,62] Our results showed that the compressive strength and modulus of PLA/nano β-TCP composite scaffolds decreased, as compared with those of pure PLA scaffolds, but were similar to the compressive strength of human cancellous bone.[34] The in vitro performance of the two scaffolds prepared in this study encouraged us to further investigate their ability to reconstruct bones in vivo. The in vivo studies on the rabbit femur bone defect model showed that the PLA/nano β-TCP composite scaffold group was significantly superior to the pure PLA group in terms of new bone regeneration, collagen content, and MD and BV/TV values. The results of osteogenesis and bone repair in vivo were similar to those reported in previous studies.[40]

The characteristics of FDM-3D-printed PLA/nano β-TCP composite scaffolds were investigated in vitro and in vivo, revealing its superior biocompatibility and good osteogenic potential. The data obtained from this study adds to the understanding of the FDM-3D printing of PLA/nano β-TCP composite scaffolds as biomaterials for bone tissue engineering, suggesting that FDM-3D printing may eventually be used to produce personalized biomaterials. However, owing to the high-temperature processing method used in FDM-3D printing, adding bioactive substances to raw materials leads to their inactivation due to the high temperature.[63] In the future, stem cells, active proteins, or drugs will be loaded into the developed FDM-3D printing composite materials,[64–67] or the composite scaffolds will be optimized using a coating to play a greater role in bone tissue repair.

Conclusion

FDM-3D-printed PLA/nano β-TCP composite scaffolds were used for bone tissue regeneration. The PLA/nano β-TCP composite scaffolds with a ratio of 7:3 prepared using FDM-3D printing exhibited good personalized porosity and shape, and their osteogenic ability, biocompatibility, and bone repair ability were superior to those of pure PLA. The merits of biodegradable PLA and bioactive nano β-TCP ceramics were combined to improve the overall biological performance of the composites. The data obtained from this study adds to the understanding of the FDM-3D printing of PLA/nano β-TCP composite scaffolds as biomaterials for bone tissue engineering, suggesting that FDM-3D printing may eventually be used to produce personalized biomaterials. This study provides a promising strategy for treating large bone defects. However, improved biological osteogenic materials are still under investigation.

Abbreviations

PLA, polylactic acid; 3D, three-dimensional; FDM, Fused deposition modeling; TCP, tricalcium phosphate; CAD, computer-aided drafting; SEM, scanning electron microscopy; EDS, energy-dispersive X-ray spectroscopy; FTIR,

Fourier-transform infrared; WCA, water contact angle; BMMSC, bone marrow mesenchymal stem cells; DMEM, Dulbecco's modified Eagle's medium; CLSM, confocal laser scanning microscopy; PFA, paraformaldehyde; PBS, phosphate buffered saline; FITC, fluorescein isothiocyanate; DAPI, 4′,6-diamidino-2-phenylindole; ALP, alkaline phosphatase; OCN, osteocalcin; COL1, collagen I; H&E, hematoxylin and eosin; micro-CT, micro-computed tomography; MD, mineral density; BV, bone tissue volume, TV, total volume; PEEK, polyetheretherketone.

Acknowledgments

This work was partially supported by Science and Technology Project of Tibet Autonomous Region (XZ202202YD0013C, XZ202102YD0026C); Sichuan Science and Technology Program (2021YJ0135, 2023YFQ0053); Project of Sichuan Provincial Department of Science and Technology (2022JDRC0133); Foundation of The First Affiliated Hospital of Chengdu Medical College (CYFY-GQ35); Foundation of Chengdu Medical College (CYZYB21-12); Special Research Project of Sichuan Medical Association (Hengrui) Scientific Research Fund (2021HR56).

Disclosure

The authors report no conflicts of interest in this work.

References

1. Mohammadi M, Mousavi Shaegh SA, Alibolandi M, et al. Micro and nanotechnologies for bone regeneration: recent advances and emerging designs. *J Control Release*. 2018;274:35–55. doi:10.1016/j.jconrel.2018.01.032
2. Zhang Z, Liu P, Wang W, et al. Epidemiology and Drug Resistance of Fracture-Related Infection of the Long Bones of the Extremities: a Retrospective Study at the Largest Trauma Center in Southwest China. *Front Microbiol*. 2022;13:923735. doi:10.3389/fmicb.2022.923735
3. Archunan MW, Petronis S. Bone Grafts in Trauma and Orthopaedics. *Cureus*. 2021;13(9):e17705. doi:10.7759/cureus.17705
4. Schmidt AH. Autologous bone graft: is it still the gold standard? *Injury*. 2021;52 Suppl 2:S18–S22. doi:10.1016/j.injury.2021.01.043
5. Leng Y, Ren G, Cui Y, et al. Platelet-rich plasma-enhanced osseointegration of decellularized bone matrix in critical-size radial defects in rabbits. *Ann Transl Med*. 2020;8(5):198. doi:10.21037/atm.2020.01.53
6. Dimitriou R, Jones E, McGonagle D, Giannoudis PV. Bone regeneration: current concepts and future directions. *BMC Med*. 2011;9:66. doi:10.1186/1741-7015-9-66
7. Feng X, Ma L, Liang H, et al. Osteointegration of 3D-Printed Fully Porous Polyetheretherketone Scaffolds with Different Pore Sizes. *ACS Omega*. 2020;5(41):26655–26666. doi:10.1021/acsomega.0c03489
8. Maghsoudlou MA, Nassireslami E, Saber-Samandari S, Khandan A. Bone Regeneration Using Bio-Nanocomposite Tissue Reinforced with Bioactive Nanoparticles for Femoral Defect Applications in Medicine. *Avicenna J Med Biotechnol*. 2020;12(2):68–76.
9. Kim Y, Park EJ, Kim TW. Recent Progress in Drug Release Testing Methods of Biopolymeric Particulate System. *Pharmaceutics*. 2021;13(8). doi:10.3390/pharmaceutics13081313
10. Vlachopoulos A, Karlioti G, Balla E, et al. Poly(Lactic Acid)-Based Microparticles for Drug Delivery Applications: an Overview of Recent Advances. *Pharmaceutics*. 2022;14(2). doi:10.3390/pharmaceutics14020359
11. Perez Davila S, Gonzalez Rodriguez L, Chiussi S, Serra J, Gonzalez P. How to Sterilize Polylactic Acid Based Medical Devices? *Polymers*. 2021;13(13). doi:10.3390/polym13132115
12. Jia L, Zhang P, Ci Z, et al. Immune-Inflammatory Responses of an Acellular Cartilage Matrix Biomimetic Scaffold in a Xenotransplantation Goat Model for Cartilage Tissue Engineering. *Front Bioeng Biotechnol*. 2021;9:667161. doi:10.3389/fbioe.2021.667161
13. Han SH, Cha M, Jin YZ, Lee KM, Lee JH. BMP-2 and hMSC dual delivery onto 3D printed PLA-Biogel scaffold for critical-size bone defect regeneration in rabbit tibia. *Biomed Mater*. 2020;16(1):015019. doi:10.1088/1748-605X/aba879
14. Eliaz N, Metoki N. Calcium Phosphate Bioceramics: a Review of Their History, Structure, Properties, Coating Technologies and Biomedical Applications. *Materials*. 2017;10(4). doi:10.3390/ma10040334
15. Hou X, Zhang L, Zhou Z, et al. Calcium Phosphate-Based Biomaterials for Bone Repair. *J Funct Biomater*. 2022;13(4). doi:10.3390/jfb13040187
16. Kang HJ, Makkar P, Padalhin AR, Lee GH, Im SB, Lee BT. Comparative study on biodegradation and biocompatibility of multichannel calcium phosphate based bone substitutes. *Mater Sci Eng C Mater Biol Appl*. 2020;110:110694. doi:10.1016/j.msec.2020.110694
17. Jeong J, Kim JH, Shim JH, Hwang NS, Heo CY. Bioactive calcium phosphate materials and applications in bone regeneration. *Biomater Res*. 2019;23:4. doi:10.1186/s40824-018-0149-3
18. Jiao X, Sun X, Li W, et al. 3D-Printed beta-Tricalcium Phosphate Scaffolds Promote Osteogenic Differentiation of Bone Marrow-Deprived Mesenchymal Stem Cells in an N6-methyladenosine-Dependent Manner. *Int J Bioprint*. 2022;8(2):544. doi:10.18063/ijb.v8i2.544
19. Liang L, Rulis P, Ching WY. Mechanical properties, electronic structure and bonding of alpha- and beta-tricalcium phosphates with surface characterization. *Acta Biomater*. 2010;6(9):3763–3771. doi:10.1016/j.actbio.2010.03.033
20. Montelongo SA, Chiou G, Ong JL, Bizios R, Guda T. Development of bioinks for 3D printing microporous, sintered calcium phosphate scaffolds. *J Mater Sci Mater Med*. 2021;32(8):94. doi:10.1007/s10856-021-06569-9
21. Joshi MK, Lee S, Tiwari AP, et al. Integrated design and fabrication strategies for biomechanically and biologically functional PLA/beta-TCP nanofiber reinforced GelMA scaffold for tissue engineering applications. *Int J Biol Macromol*. 2020;164:976–985. doi:10.1016/j.ijbiomac.2020.07.179

22. Khan Y, Yaszemski MJ, Mikos AG, Laurencin CT. Tissue engineering of bone: material and matrix considerations. *J Bone Joint Surg Am*. 2008;90 (Suppl 1):36–42. doi:10.2106/JBJS.G.01260
23. Qiao K, Xu L, Tang J, et al. The advances in nanomedicine for bone and cartilage repair. *J Nanobiotechnology*. 2022;20(1):141. doi:10.1186/s12951-022-01342-8
24. Sahmani S, Saber-Samandari S, Khandan A, Aghdam MM. Nonlinear resonance investigation of nanoclay based bio-nanocomposite scaffolds with enhanced properties for bone substitute applications. *J Alloys Compd*. 2019;773:636–653. doi:10.1016/j.jallcom.2018.09.211
25. Chen C, Huang B, Liu Y, Liu F, Lee IS. Functional engineering strategies of 3D printed implants for hard tissue replacement. *Regen Biomater*. 2023;10:rbac094. doi:10.1093/rb/rbac094
26. Zhang L, Forgham H, Shen A, et al. Nanomaterial integrated 3D printing for biomedical applications. *J Mater Chem B*. 2022;10(37):7473–7490. doi:10.1039/d2tb00931e
27. Raisi A, Asefnejad A, Shahali M, et al. A soft tissue fabricated using a freeze-drying technique with carboxymethyl chitosan and nanoparticles for promoting effects on wound healing. *J Nanoanalysis*. 2020;7(4):262–274. doi:10.22034/jna.2022.680836
28. Bardot M, Schulz MD. Biodegradable Poly(Lactic Acid) Nanocomposites for Fused Deposition Modeling 3D Printing. *Nanomaterials*. 2020;10 (12). doi:10.3390/nano10122567
29. Bandari S, Nyavanandi D, Dumpa N, Repka MA. Coupling hot melt extrusion and fused deposition modeling: critical properties for successful performance. *Adv Drug Deliv Rev*. 2021;172:52–63. doi:10.1016/j.addr.2021.02.006
30. Huang S, Wei H, Li D. Additive manufacturing technologies in the oral implant clinic: a review of current applications and progress. *Front Bioeng Biotechnol*. 2023;11:1100155. doi:10.3389/fbioe.2023.1100155
31. Wang W, Zhang B, Zhao L, et al. Fabrication and properties of PLA/nano-HA composite scaffolds with balanced mechanical properties and biological functions for bone tissue engineering application. *Nanotechnol Rev*. 2021;10(1):1359–1373.
32. Wang W, Zhang B, Li M, et al. 3D printing of PLA/n-HA composite scaffolds with customized mechanical properties and biological functions for bone tissue engineering. *Composites Part B: Eng*. 2021;224:109192.
33. Jones JR, Ehrenfried LM, Hench LL. Optimising bioactive glass scaffolds for bone tissue engineering. *Biomaterials*. 2006;27(7):964–973. doi:10.1016/j.biomaterials.2005.07.017
34. Zhang B, Wang L, Song P, et al. 3D printed bone tissue regenerative PLA/HA scaffolds with comprehensive performance optimizations. *Mater Des*. 2021;201:109490.
35. Wu T, Yu S, Chen D, Wang Y. Bionic Design, Materials and Performance of Bone Tissue Scaffolds. *Materials*. 2017;10(10). doi:10.3390/ma10101187
36. Zhou C, Wang K, Sun Y, et al. Biofabrication (3D bioprinting) laboratory at Sichuan University. *Bio-Design and Manufacturing*. 2021;4:432–439.
37. Song P, Li M, Zhang B, et al. DLP fabricating of precision GelMA/HAp porous composite scaffold for bone tissue engineering application. *Composites Part B: Eng*. 2022;244:110163.
38. Ozada KA. Novel Microstructure Mechanical Activated Nano Composites for Tissue Engineering Applications. *J Bioengineering Biomed Sci*. 2015;05(01). doi:10.4172/2155-9538.1000143
39. Bohner M, Santoni BLG, Dobelin N. beta-tricalcium phosphate for bone substitution: synthesis and properties. *Acta Biomater*. 2020;113:23–41. doi:10.1016/j.actbio.2020.06.022
40. Cao L, Duan PG, Wang HR, et al. Degradation and osteogenic potential of a novel poly(lactic acid)/nano-sized beta-tricalcium phosphate scaffold. *Int J Nanomedicine*. 2012;7:5881–5888. doi:10.2147/IJN.S38127
41. Wu L, Zhou C, Zhang B, et al. Construction of biomimetic natural wood hierarchical porous-structure bioceramic with micro/nanowhisker coating to modulate cellular behavior and osteoinductive activity. *ACS Appl Mater Interfaces*. 2020;12(43):48395–48407.
42. Majhy B, Priyadarshini P, Sen AK. Effect of surface energy and roughness on cell adhesion and growth - facile surface modification for enhanced cell culture. *RSC Adv*. 2021;11(25):15467–15476. doi:10.1039/d1ra02402g
43. Wang W, Wei J, Lei D, et al. 3D printing of lithium osteogenic bioactive composite scaffold for enhanced bone regeneration. *Composites Part B: Eng*. 2023;110641.
44. Lin KF, He S, Song Y, et al. Low-Temperature Additive Manufacturing of Biomimic Three-Dimensional Hydroxyapatite/Collagen Scaffolds for Bone Regeneration. *ACS Appl Mater Interfaces*. 2016;8(11):6905–6916. doi:10.1021/acsami.6b00815
45. Moarrefzadeh A, Morovvati MR, Angili SN, Smaisim GF, Khandan A, Toghraie D. Fabrication and finite element simulation of 3D printed poly L-lactic acid scaffolds coated with alginate/carbon nanotubes for bone engineering applications. *Int J Biol Macromol*. 2023;224:1496–1508. doi:10.1016/j.ijbiomac.2022.10.238
46. Wubneh A, Tsekoura EK, Ayranci C, Uludag H. Current state of fabrication technologies and materials for bone tissue engineering. *Acta Biomater*. 2018;80:1–30. doi:10.1016/j.actbio.2018.09.031
47. Fan HS, Wen XT, Tan YF, Wang R, Cao H, Zhang XD. Compare of electrospinning PLA and PLA/β-TCP scaffold in vitro. *Trans Tech Publ*. 2005;2379–2382.
48. Perez-Davila S, Gonzalez-Rodriguez L, Lama R, et al. 3D-Printed PLA Medical Devices: physicochemical Changes and Biological Response after Sterilisation Treatments. *Polymers*. 2022;14(19). doi:10.3390/polym14194117
49. Lou CW, Yao CH, Chen YS, et al. PLA/ beta-TCP complex tubes: the mechanical properties and applications of artificial bone. *J Biomater Sci Polym Ed*. 2012;23(13):1701–1712. doi:10.1163/092050611X597762
50. Elhattab K, Bhaduri SB, Sikder P. Influence of Fused Deposition Modelling Nozzle Temperature on the Rheology and Mechanical Properties of 3D Printed beta-Tricalcium Phosphate (TCP)/Polylactic Acid (PLA) Composite. *Polymers*. 2022;14(6). doi:10.3390/polym14061222
51. Tang D, Tare RS, Yang LY, Williams DF, Ou KL, Oreffo RO. Biofabrication of bone tissue: approaches, challenges and translation for bone regeneration. *Biomaterials*. 2016;83:363–382. doi:10.1016/j.biomaterials.2016.01.024
52. Chandorkar Y, Bhaskar N, Madras G, Basu B. Long-term sustained release of salicylic acid from cross-linked biodegradable polyester induces a reduced foreign body response in mice. *Biomacromolecules*. 2015;16(2):636–649. doi:10.1021/bm5017282
53. Kang Y, Yao Y, Yin G, et al. A study on the in vitro degradation properties of poly(L-lactic acid)/beta-tricalcuim phosphate (PLLA/beta-TCP) scaffold under dynamic loading. *Med Eng Phys*. 2009;31(5):589–594. doi:10.1016/j.medengphy.2008.11.014

54. Araque-Monros MC, Gamboa-Martinez TC, Santos LG, Bernabe SG, Pradas MM, Estelles JM. New concept for a regenerative and resorbable prosthesis for tendon and ligament: physicochemical and biological characterization of PLA-braided biomaterial. *J Biomed Mater Res A*. 2013;101(11):3228–3237. doi:10.1002/jbm.a.34633
55. Manolagas SC. Osteocalcin promotes bone mineralization but is not a hormone. *PLoS Genet*. 2020;16(6):e1008714. doi:10.1371/journal.pgen.1008714
56. Liu X, Zheng C, Luo X, Wang X, Jiang H. Recent advances of collagen-based biomaterials: multi-hierarchical structure, modification and biomedical applications. *Mater Sci Eng C Mater Biol Appl*. 2019;99:1509–1522. doi:10.1016/j.msec.2019.02.070
57. Chen Y, Yang S, Lovisa S, et al. Type-I collagen produced by distinct fibroblast lineages reveals specific function during embryogenesis and Osteogenesis Imperfecta. *Nat Commun*. 2021;12(1):7199. doi:10.1038/s41467-021-27563-3
58. Zhang H, Mao X, Du Z, et al. Three dimensional printed macroporous polylactic acid/hydroxyapatite composite scaffolds for promoting bone formation in a critical-size rat calvarial defect model. *Sci Technol Adv Mater*. 2016;17(1):136–148. doi:10.1080/14686996.2016.1145532
59. Haimi S, Suuriniemi N, Haaparanta AM, et al. Growth and osteogenic differentiation of adipose stem cells on PLA/bioactive glass and PLA/beta-TCP scaffolds. *Tissue Eng Part A*. 2009;15(7):1473–1480. doi:10.1089/ten.tea.2008.0241
60. Liu T, Li B, Chen G, Ye X, Zhang Y. Nano tantalum-coated 3D printed porous polylactic acid/beta-tricalcium phosphate scaffolds with enhanced biological properties for guided bone regeneration. *Int J Biol Macromol*. 2022;221:371–380. doi:10.1016/j.ijbiomac.2022.09.003
61. Cao L, Duan PG, Li XL, et al. Biomechanical stability of a bioabsorbable self-retaining polylactic acid/nano-sized beta-tricalcium phosphate cervical spine interbody fusion device in single-level anterior cervical discectomy and fusion sheep models. *Int J Nanomedicine*. 2012;7:5875–5880. doi:10.2147/IJN.S38288
62. Cao L, Chen Q, Jiang LB, et al. Bioabsorbable self-retaining PLA/nano-sized beta-TCP cervical spine interbody fusion cage in goat models: an in vivo study. *Int J Nanomedicine*. 2017;12:7197–7205. doi:10.2147/IJN.S132041
63. Iranmanesh P, Ehsani A, Khademi A, et al. Application of 3D Bioprinters for Dental Pulp Regeneration and Tissue Engineering (Porous architecture). *Transport in Porous Media*. 2022;142(1):265–293. doi:10.1007/s11242-021-01618-x
64. Zhang B, Wang W, Gui X, et al. 3D printing of customized key biomaterials genomics for bone regeneration. *Applied Materials Today*. 2022;26:101346.
65. Li M, Song P, Wang W, et al. Preparation and characterization of biomimetic gradient multi-layer cell-laden scaffolds for osteochondral integrated repair. *J Materials Chem B*. 2022;10(22):4172–4188.
66. Iranmanesh P, Gowdini M, Khademi A, et al. Bioprinting of three-dimensional scaffold based on alginate-gelatin as soft and hard tissue regeneration. *J Materials Res Technol*. 2021;14:2853–2864. doi:10.1016/j.jmrt.2021.08.069
67. Soleimani M, Asgharzadeh Salmasi A, Asghari S, et al. Optimization and fabrication of alginate scaffold for alveolar bone regeneration with sufficient drug release. *International Nano Letters*. 2021;11(3):295–305. doi:10.1007/s40089-021-00342-0